ACS APPLIED MATERIALS & INTERFACES

Research Article

www.acsami.org

Large Surface Area Ordered Porous Carbons via Nanocasting Zeolite 10X and High Performance for Hydrogen Storage Application

Jinjun Cai,[†,‡] Liangjun Li,[†,‡] Xiaoxia Lv,[†,‡] Chunpeng Yang,[†] and Xuebo Zhao*[,†]

[†]Qingdao Institute of Bioenergy and Bioprocess Technology, Chinese Academy of Sciences, Qingdao 266101, People's Republic of China

[‡]University of Chinese Academy of Sciences, Beijing 100049, People's Republic of China

Supporting Information

ABSTRACT: We report the preparation of ordered porous carbons for the first time via nanocasting zeolite 10X with an aim to evaluate their potential application for hydrogen storage. The synthesized carbons exhibit large Brunauer-Emmett-Teller surface areas in the 1300−3331 m^2/g range and pore volumes up to 1.94 cm^3/g with a pore size centered at 1.2 nm. The effects of different synthesis processes with pyrolysis temperature varied in the 600−800 °C range on the surface areas, and pore structures of carbons were explored. During the carbonization process, carbons derived from the liquid−gas two-step routes at around 700 °C are nongraphitic and retain the particle morphology of 10X zeolite, whereas the higher pyrolysis temperature results in some graphitic domains and hollow-shell morphologies. In contrast, carbons derived from the direct acetylene infiltration process have some incident nanoribbon or nanofiber morphologies. A considerable hydrogen storage capacity of 6.1 wt % at 77 K and 20 bar was attained for the carbon with the surface area up to 3331 m^2/g, one of the top-ranked capacities ever observed for large surface area adsorbents, demonstrating their potential uses for compacting gaseous fuels of hydrogen. The hydrogen capacity is comparable to those of previously reported values on other kinds of carbon-based materials and highly dependent on the surface area and micropore volume of carbons related to the optimum pore size, therefore providing guidance for the further search of nanoporous materials for hydrogen storage.

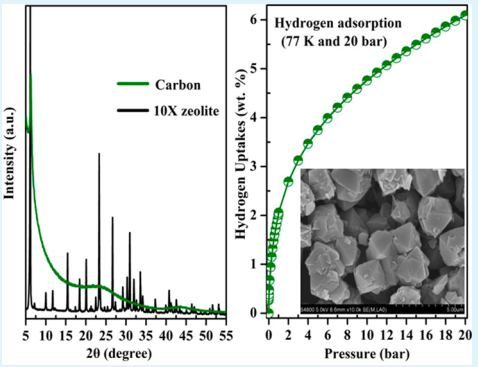

KEYWORDS: *porous carbons, adsorption, nanocasting, zeolite template, hydrogen storage*

INTRODUCTION

Recently, hydrogen as an alternative to fossil fuel has been recognized as an attractive energy carrier and fuel in the near future because it has high energy densities and creates neither air pollution nor greenhouse gas emissions.[1−3] The main drawback for hydrogen as a transportation fuel is the lack of an effective storage method, which is yet to reach the criterions set by the DOE (Department of Energy, USA) for on-board application. Hence the development of cost-effective and feasible materials to satisfy on-board application claim for hydrogen storage is a great challenge.[4−7] Up to now, large numbers of adsorbents have been under intensive studies for hydrogen storage, and porous carbons with high surface areas and large pore volumes are considered as promising candidates for application as the hydrogen storage media.[8−12] The wide pore size distributions (PSDs) of conventional activated carbons in both the micro- and mesopore ranges will greatly affect their storage performance.[13] Therefore, it is not difficult to imagine that preparation of carbons with a narrow PSD is very important in determining their adsorption performance. The template carbonization route is a versatile and well fitted methodology for the preparation of porous materials especially for the carbon-based materials with a controlled architecture and relative narrow PSD.[11,14−16] The template method usually involves first filling the nanopores of a solid (as the template) with a different material (as the precursor), followed by the chemical separation of these resulting materials from the used template. Indeed, using inorganic materials with regular nanospaces as the hard template will effectively instruct the formation of pores during carbonization and further improve the level of structural orderings. Many works have demonstrated that this template route offers a rigid nanocasting mold to replicate porous carbons with a controlled pore structure.[11,14] There is no doubt that the sensible choice of templates or precursors is one of the most critical issues for preparing carbons with superior performance in their potential applications, especially for the hydrogen storage.

Zeolites with well-defined nanopores are good candidates for preparing ordered carbons, and some excellent reviews available in literatures have fully reviewed the fields of template method for preparing ordered micro- or mesoporous carbons.[11,14,17−19] For example, Kyotani's group performed lots of pioneering works on ordered microporous carbons and indicated that zeolite Y possessed the best transferability in the structural

Received: September 4, 2013
Accepted: December 17, 2013
Published: December 17, 2013

Scheme 1. Schematic Illustration of the Preparation Procedure for Generating Carbons via Nanocasting Method Using 10X Zeolite As the Template

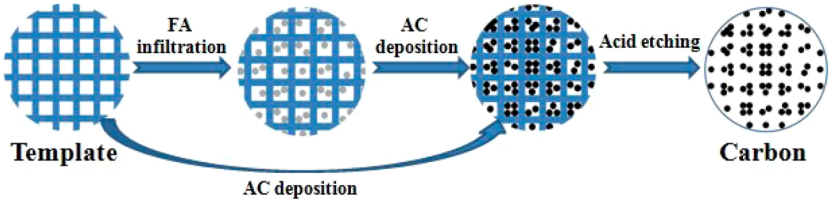

orderings due to its three-dimensional nanopores and suitable pore size compared to other kinds of zeolites such as ß, L, ZSM-5, and mordenite.[17,20] Furthermore, previous investigations have also suggested that the preparation parameters such as nature of precursor, temperature, and deposition time can largely affect the textural properties of carbons, especially for pore size and porosity.[21−26] The optimal conditions can be greatly different even though the template of similar pore size and topology is used.[27] All previous reported data have indicated the promising potential of this template-synthesis method in hydrogen storage.[11] On the other hand, if the molecular size of precursor is slightly smaller than the inner pore channels of adopted zeolites, the diffusion of precursor gas into its internal nanopores would be much easier, and the precursor gas could go inside without serious deposition on the external surface of zeolites.[28] To date, commercial zeolites including Y with different cations, ß, 13X, and synthetic zeolites (e.g., EMC-2) have been experimentally used as templates to fabricate ordered microporous carbons for hydrogen storage.[11,14] As we all know that the X zeolite usually has a larger pore width than Y zeolite, it will certainly make the nanocasting process much easier. However, the preparation of porous carbons via nanocasting 10X zeolite, which also has three-dimensional interconnected nanopores, to the best of our knowledge, has not been reported yet.

Herein, we performed an extensive investigation for the first time on the preparation of ordered porous carbons using 10X zeolite as the hard template. The resulting carbons possess an ordered nanostructure, large surface area, high microporosity, and a controlled narrow PSD. As one of the promising applications for porous carbons is hydrogen storage, combining the two facts that some scholars have previously reported exciting data at low temperature collected on similar carbons,[29−40] and the 10X zeolite has never been used as the hard template for the nanocasting, to the best of our knowledge, we are greatly interested in the relationship between the pore structure of the carbons and adsorption properties of hydrogen. Although there are large numbers of exciting data for hydrogen at 77 K on these ordered zeolite-templated carbons and some activated carbons,[29,41] on the other hand, we also must note that there is still great controversy and doubt, even errors, about the actual hydrogen capacity on these related carbon-based materials, especially for high pressures adsorption, resulting from an inaccuracy of inherent buoyancy effect during measurements on gravimetric equipment. Furthermore, we believe that detailed studies for hydrogen storage are very necessary and will be interesting in view of abundant microporisity existed in carbons. Therefore, we evaluated the adsorption performance of hydrogen at 77 K on carbons up to 20 bar with full consideration of buoyancy effect and provided some additional insights into the crucial effects of pore structure on the hydrogen storage in carbons.

EXPERIMENTAL SECTION

Reagents and Carbon Preparation. The 10X zeolite (SiO_2/Al_2O_3 = 2.6−3.0, Jianlong Chem. Co., Ltd., China) was selected as template after precalcination at 550 °C for 6 h in air. On the basis of the information provided by the manufacturer, an exchange degree for calcium ion is 75%. Furfuryl alcohol (FA, 98%, Sinopharm Chemical Reagent Co., Ltd,) and acetylene (AC, Heli Gas Co., Ltd., China) were chosen as precursors. Scheme 1 illustrates the preparation process for porous carbons via nanocasting routes, and the detailed procedures can also be found elsewhere[20,42] with some modification in the etching process. Briefly, powdery 10X zeolite impregnated with FA was heated at 80 °C for 24 h and 150 °C for 8 h in a N_2 flow. The composites were settled in a vertical quartz tube (i.d. = 16 mm) and heated up to a deposition temperature (600−800 °C) at a rate of 5 °C/min under a N_2 flow. Once the desired temperature was reached, the gas was immediately changed to a mixture of N_2/C_2H_2 (95:5, volume ratio) at 100 mL/min for 4 h to deposit carbons onto zeolite. For comparison, two carbons were prepared via a direct acetylene deposition at 600 °C for 4 h and 700 °C for 1 h or at 700 °C for 5 h. Finally, the zeolite−carbon composites were continually heated at 900 °C for 3 h, and then zeolite was dissolved by refluxing in concentrated HCl at 60 °C for 3.5 h and washing with 40% HF at room temperature for 6 h. An opposite sequence for the etching will not work due to the formation of insoluble calcium fluoride. Carbons was separated by filtration and washed with copious of distilled water and dried at 120 °C overnight.

Carbons derived from the liquid−gas two-step routes were denoted as 10Xc-60, 10Xc-65, 10Xc-70, 10Xc-75, and 10Xc-80, corresponding to a CVD temperature of 600, 650, 700, 750, and 800 °C, respectively. In addition, the carbon derived from direct infiltration of acetylene at 600 °C for 4 h and 700 °C for 1 h was denoted as 10Xc60-7S, and the carbon obtained from the acetylene pyrolysis at 700 °C for 5 h was denoted as 10Xc-70S.

Characterization of Carbons. The structural features of carbons were investigated via the X-ray diffractometer (XRD, Bruker D8 Advance). The morphological analysis was performed with the observations on scanning electron microscopy (SEM, Hitachi S4800, 5 kV) and high-resolution transmission electron microscopy (HRTEM, JEOL, JEM-2010, 200 kV). The contents of C/H in the bulk carbons were measured with an automatic analyzer (Elementar Vario EL), and the contents of O element were calculated by difference. N_2 sorption measurements were carried out at 77 K on a static volumetric sorption analyzer (ASAP2020, Micrometrics, USA). Surface area was calculated using the Brunauer−Emmett−Teller (BET) method based on adsorption data of N_2 in a relative pressure (P/P_0) range of 0.02−0.25, which was selected taking into account a previous report that a lower partial pressure range (0.01−0.05) overestimates surface area whereas a higher partial pressure range (0.1−0.3) underestimates surface area.[40] In addition, we have calculated surface area using the density functional theory (DFT) method,[43,44] which is also a promising method for the characterization of microporous carbons. Before the adsorption measurement, samples were evacuated for 15 h at 200 °C under high vacuum.

Hydrogen Uptake Measurements. Hydrogen sorption measurements were performed on an Intelligent Gravimetric Analyzer (IGA-001, Hiden, UK) which is an ultrahigh vacuum system and incorporates a microbalance capable of measuring weights with a resolution of ±0.1 μg. To facilitate the confirmation of our hydrogen sorption results, deuterium sorption at 1 bar was also measured for

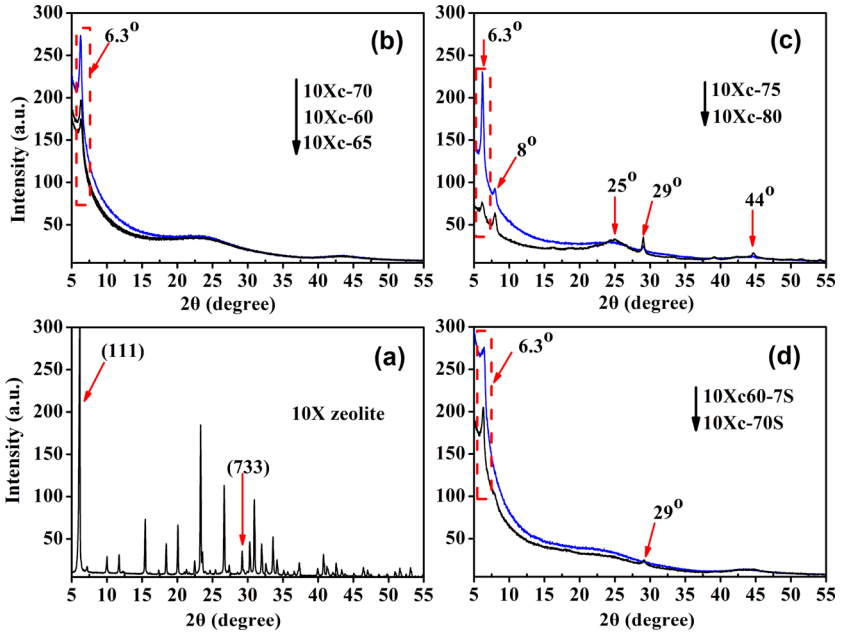

Figure 1. Typical XRD patterns for (a) the 10X zeolite template, (b, c) carbons obtained from the liquid−gas two step routes (10Xc-60, 10Xc-65, 10Xc-70, 10Xc-75, and 10Xc-80), and (d) carbons obtained from the single acetylene deposition process (10Xc60-7S and 10Xc-70S).

comparison on the IGA. Ultrahigh-purity (99.9999%) hydrogen and high-purity (99.5%) deuterium were used for adsorption measurement and the two gases were further purified with the activated alumina, zeolites, and activated carbons to remove probable trace amount of water and other impurities before introduction into IGA system. Importantly, the skeleton density of 1.5 g/cm^3 and total pore volume obtained from N_2 adsorption for carbons were used for the buoyancy corrections of the adsorbed hydrogen. Before sorption measurements, samples were degassed (10^{-6} bar) at 200 °C for 3 h, with a heating rate of 1 °C/min.

RESULTS AND DISCUSSION

XRD patterns of porous carbons obtained from different preparation routes using zeolite 10X as hard template are shown in Figure 1. For comparison, the XRD pattern of original 10X zeolite template is also included (see Figure 1a). It is clear that each carbon, regardless of the liquid−gas two-step routes or the single gas CVD process, shows a sharp diffraction at around $2\theta = 6.3°$ (hereinafter referred to as "basal peak"). The basal peak is believed originating from the (111) plane of 10X zeolite, indicating that some of structural regularity with periodicity of about 1.4 nm exists in carbons.[20,42] This feature is in good agreement with the reported data using other kinds of zeolite as the template.[29,32−34,40,45−49] It is observed that the pyrolysis temperature and preparation routes are very critical to the intensity of the basal peak, and the intensity for the liquid−gas two-step routes is obviously stronger than the ones for a single gas CVD process. Admittedly, the phenomenon indicates that impregnating some precursor into the nanopores of 10X zeolite during the preliminary carbonization process is very beneficial for acquiring carbons with high structural orderings. Furthermore, two broad and weak peaks are observed at around 25 and 44° in all carbons although their intensities have some difference, attributing to the (002) and (100) plane from turbostratic carbons, respectively.[20,42] The disappearance of other zeolite diffractions confirmed that the template removal process was a success. We found that the higher temperature for the precursor pyrolysis is, the larger proportion of graphitization in the carbon inherits (see Figure 1b,c). However, the graphitic degree of all these carbons was poor even at elevated temperatures and most of them are amorphous. The overall broadening and low-intensity for the (002) diffraction also indicate that these carbons are essentially amorphous structures (e.g., nongraphitic) and most of the precursors are deposited inside the pores of 10X zeolite rather than on the external surface. If not, precursors would experience great graphitization and then formation of some stacked graphene sheets due to the absence of spatial limitations on the zeolite surface.[28,40,48] On the other hand, it is worth noting that two weak but relatively sharp diffraction peaks at around 8 and 29° are observed for the first time in the following three samples: 10Xc-75, 10Xc-80, and 10Xc-70S (see Figure 1c,d). We spontaneously deduce that the peak at around 8° belongs to other turbostratic carbons (e.g., C_{60}) in view of the following reasons: (1) an increase of the peak intensity results in a decrease in the intensity of basal peak, and (2) no other diffraction peak is found at the corresponding location in the parent X zeolite. In contrast, the diffraction at around 29° is located at a position similar to that of the (733) plane of 10X zeolite although its intensity in zeolite is much weaker than the (111) plane, and we speculatively attribute this peak to the zeolite-structural ordering even though we cannot rule out the possibility that the diffraction maybe also arise from other turbostratic or graphite carbon contaminants.[33,40] The overall XRD patterns indicate that 10X zeolite is successfully applied as the hard template to nanocast porous carbons, and the long-range structural ordering of the carbons is confidently transferred from the original 10X zeolite template.

The morphologies of 10X zeolites and carbons are confirmed by the SEM analysis and the corresponding images are shown in Figure 2. It is clear that the 10X zeolite shows an obvious crystal-like morphology with a size of about 1.5μm in each particle (see Figure 2a). However, the morphology of carbons inherited from the 10X zeolite varies a lot with different pyrolysis conditions. For example, the 10Xc-60 in Figure 2b partly shows a layered-graphite structure, resulting from the collapse of unstable carbon frameworks during the etching

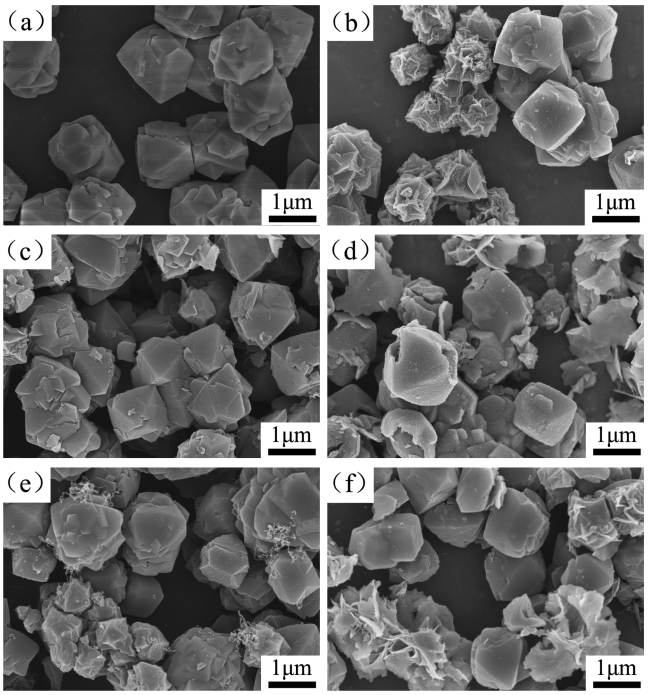

Figure 2. The representative SEM images for (a) 10X zeolite and porous carbon replicas, (b) 10Xc-60, (c) 10Xc-70, (d) 10Xc-80, (e) 10Xc60-7S, and (f) 10Xc-70S.

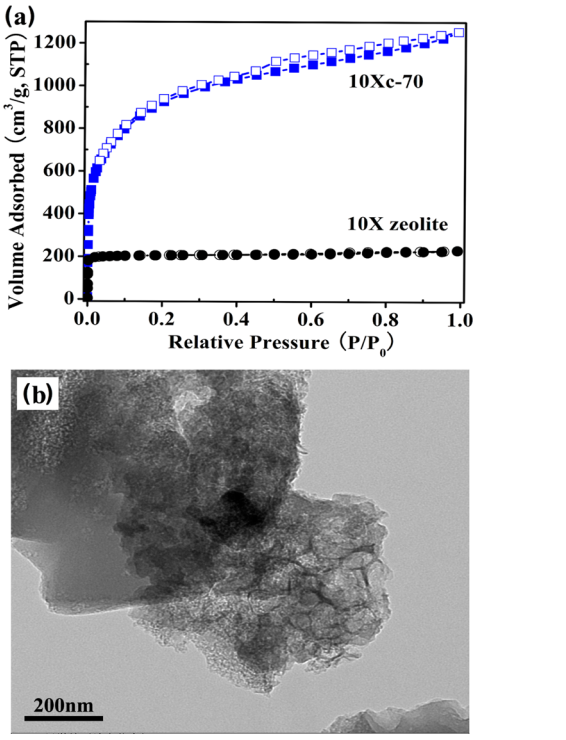

Figure 3. (a) N_2 sorption isotherms for 10X zeolite and 10Xc-70 (Ads: filled symbols; Des: open symbols) and (b) representative TEM image of 10Xc-70 carbon.

processes. The 10Xc-70 in Figure 2c displays crystal-like and sharp particle edges with a smooth surface in each particle and also accompanies some particle aggregation, indicating that the precursor is mostly deposited inside the nanopores of 10X zeolites during acetylene CVD process even though there maybe a little deposition on the surface of zeolites.[20,28,34] On the other hand, the 10Xc-80 in Figure 2d shows much rougher surface with some hollow-shell and graphitic nanosheets, indicating that a serious carbon precursor deposition on the external surface of 10X zeolite occurs because of the accelerated carbonization process at higher pyrolysis temperatures.[34,48] In addition, it should be noted that the 10Xc60-7S and 10Xc-70S (Figure 2e,f, respectively) obtained from single acetylene CVD process also show obvious crystal-like morphology but contain some accessory graphitic nanoribbons and nanosheets, reflecting a lower diffraction intensity for the basal peak in Figure 1d. The SEM images are consistent with the XRD data in Figure 1 with respect to the graphitic or amorphous nature of the carbons, and we attribute the interesting phenomena that the presence of some hybrid nanostructures derived from single acetylene deposition partly to catalytic effects on the surface of 10X zeolite. Carbons derived from certain conditions exhibit and resemble a crystal-like morphology coupled with a particle size almost comparable to the 10X zeolite, providing important supporting evidence for this template-synthesis mechanism that the precursor is predominantly nanocast within the nanopores of the template and the obtained carbons are wholly negative replicas of the 10X zeolite particles.

The N_2 sorption isotherms for the 10X zeolite template and representative 10Xc-70 carbon is depicted in Figure 3a and their detailed structural parameters are summarized in the Table 1. N_2 sorption isotherms for other carbons (in Figure S1, Supporting Information) are not provided in Figure 3a because they are very similar in their shapes and trends compared to the 10Xc-70 only with some difference in adsorbed amounts. As shown in Figure 3a and S1 (Supporting Information), all the carbons adsorb large numbers of N_2 molecules at low pressure ranges ($P/P_0 < 0.05$), indicating the large proportion of microporosity. The presence of micropores is is consistent with the observed high structural ordering in the XRD patterns (Figure 1) for carbons.[20,42] It is very interesting to note that the adsorbed amounts of N_2 in carbons are much larger than ones in the 10X zeolite template. We think that the resulting N_2 adsorption isotherms for all carbons still resemble the type I isotherms according to the IUPAC classification,[50] even if the isotherms have obvious small hysteresis loops. In general, the smoother the isotherms are, the more micropores exist in carbons, and vice versa. It is very obvious that isotherms of all carbons exhibit an obvious hysteresis loop over a wide pressure range ($P/P_0 > 0.4$), suggesting the presence of both micropores and mesopores. The part of mesopores is probably due to partial collapse of carbon frameworks in view of their poor stabilities during the etching process, resulting from an incomplete infiltration of precursors in the micropore channels of 10X zeolites.[34,48,51] Similar hysteresis loops in isotherms have also previously been observed for ordered porous carbons using other kinds of zeolites as the hard template.[29,30,33,36,47] On the other hand, the representative TEM images of the 10Xc-70 in Figures 3b and S2 (Supporting Information) further demonstrate that a part of the carbon precursors does have deposits on the external surface of the 10X zeolite template, and the carbons do have some randomly distributed mesopores, which are in excellent agreement with XRD and N_2 isotherms observations.

From the pore structure parameters listed in Table 1, we can obviously find that the pore textures of carbons are largely dependent on the preparation conditions, namely, surface area and total pore volume of carbons derived from the liquid–gas

Table 1. Textural Structure Parameters and Hydrogen Storage Capacities of Carbons Derived from Different Preparation Conditions

						[e]H_2 [wt %]		[f]elemental analysis (%)		
adsorbent	[a]S_{BET} [m^2/g]	[b]S_{DFT} [m^2/g]	[c]V_{total} [cm^3/g]	[d]V_{micro} [cm^3/g]	pore sizes (Å)	1 bar	20 bar	C	H	O (diff)
10Xc-60	2236 (1535)	2144	1.35	0.67	6/8/12/20	1.83	5.12	87.11	0.92	11.97
10Xc-70	3331 (2281)	3340	1.94	1.00	6/8/12/20	2.01	6.09	89.16	1.83	9.01
10Xc-75	2366 (1532)	2418	1.44	0.69	7/12/20	1.96	5.67	88.88	0.46	10.66
10Xc-80	1303 (737)	1307	0.88	0.33	12/20	1.09	3.23	80.72	0.36	18.92
10Xc60-7S	2254 (1538)	2139	1.33	0.71	6/8/12/20	2.27	5.61	87.48	1.08	11.44
10Xc-70S	2198 (1275)	2117	1.35	0.58	6/8/12/20	1.56	5.01	84.06	0.65	15.29

[a]Surface area is calculated using the BET method at P/P_0 = 0.02−0.25, and values in parentheses are micropore surface areas calculated from the t-plot method using carbon black STPA in the range of 0.45−0.6 nm film thickness. [b]Surface area is calculated using the DFT method. [c]Total pore volume is estimated from the N_2 adsorption data at P/P_0 = 0.995. [d]Micropore volume is calculated from the t-plot method; [e]Hydrogen storage capacities at 77 K and elevated pressures are measured via the gravimetric method. [f]Element composition is calculated via temperature-programmed oxidation, and content of oxygen is calculated from the elemental analysis as a difference to 100% because ash is neglected.

two-step routes are much larger than ones from the single gas CVD process. As expected, carbons that exhibit well-developed zeolite-like orderings generally have a higher proportion of micropore surface area and pore volume.[20,28] The micropore surface areas of carbons calculated from the t-plot method are varied in the 737−2281 m^2/g range, and the micropore volume of 10Xc-70 is close to 1.0 cm^3/g, demonstrating the large proportion of microporosity in the carbons. In addition, the total pore volumes of carbons are also very large, varying between 1.33 and 1.94 cm^3/g. All the carbons except for the 10Xc-80 exhibit high BET specific surface areas in the 2100−3300 m^2/g range with more than 60% arising from micropores. The detailed calculations for the BET specific surface area of carbons are shown in Figure S3 (Supporting Information). The relatively smaller surface area and lower pore volume for the 10Xc-80 is probably due to its serious graphitization and low structure orderings compared to other carbons. In contrast, the BET surface area and total pore volume of 10Xc-70 are very comparable to that of previously reported data for carbons inherited from Y zeolite or EMC-2 and larger than that of carbons from zeolite β or 13X.[20,28−30,32,33,35−38,40,47,48,51] However, it should be admitted that the BET method in many cases overestimates the surface areas, and the data can be varied depending on the adopted pressure ranges.[40,43] Therefore, an alternative DFT method was also applied to calculate the surface areas of carbons and we can observe from Table 1 that both the results derived form the BET and DFT method are almost equal to each other, and the DFT specific surface area of 10Xc-70 is close to 3340 m^2/g. The comparison between the BET and DFT data demonstrated that using the relative pressure range of P/P_0 = 0.02−0.25 to calculate the BET specific surface area of these zeolite-templated carbons is reasonable and acceptable to some extent. All the results are in good agreement with the XRD analysis in Figure 1, illustrating that the 10Xc-70 has a higher level of zeolite-like structural ordering. Both the large micropore volumes and micropore surface areas indicate that zeolite-templated carbons are promising candidates for energy-related storage applications (e.g., hydrogen storage). Moreover, the presence of moderate mesopores indicates that the storage uptakes can be further improved in a relatively higher pressure.[32] Generally, a good infiltration of the template with precursors is very important for the quality of structural replication.[40,47] As can be seen from the results of elemental analysis in Table 1, carbons obtained from this nanocasting route contain some significant levels of oxygen even if the adopted precursors do not contain any oxygen contents such as acetylene gas. We think that most of such oxygen functionalization was introduced into the framework during etching process, as is a case for most carbons derived via the nanocasting method.[20,28,46,52,53] In addition, a small part of oxygen atoms can also result from the moisture, atmospheric oxygen or CO_2 adsorbed on the surface of carbons. All the results declared above underline the importance in producing a replication structure with a high level of zeolite-like orderings, ensuring large surface areas and high pore volumes and therefore resulting in a large storage capacity.

The pore size distribution (PSD) curves of carbons determined via applying the nonlocal density functional theory (NLDFT) method to the N_2 adsorption data, assuming slit-like pore geometry, are shown in Figure 4 and the detailed pore size

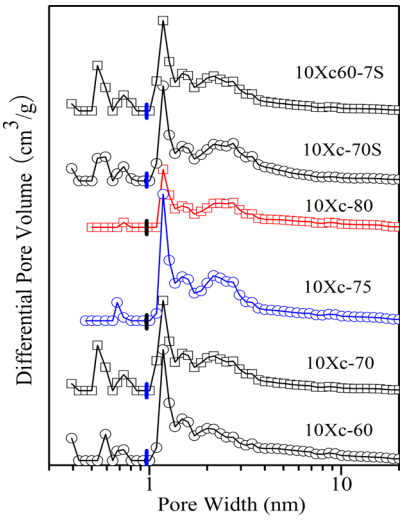

Figure 4. Pore size distribution (PSD) curves for carbons determined via applying nonlocal density functional theory (NLDFT) method to N_2 adsorption data.

is also given in Table 1. PSD curves provide more detailed information on the micropore structure of carbons. As clearly shown in Figure 4, the PSD curves for all carbons have similar shapes with a major micropore size at around 1.2 nm. Furthermore, there are some well-defined ultramicropores at less than 0.8 nm, and the presence of a small proportion of mesopores is also evidenced, corresponding to the hysteresis loop in N_2 sorption isotherms in Figure 3a. We have noted that nanopores existing at about 0.6 nm has previously been

dx.doi.org/10.1021/am403810j | ACS Appl. Mater. Interfaces 2014, 6, 167−175

reported by the group of Mokaya,[29,34,36,40,47,51,54] who demonstrated that a significant proportion of micropores at 0.6 nm is beneficial for enhancing the hydrogen storage capacities, especially for high pressures. Therefore, we have reason to believe that the carbons reported here probably also have high hydrogen storage uptakes. The contribution of ultramicropores can be attributed to the intrinsic microporosities of the carbon matrix.[23,55] Importantly, the pore size at around 1.2 nm is ascribed to the faithful replication of 10X zeolites wall as indicated by many previous studies with other zeolites.[20,28,30,42,47] As for the presence of small mesopores in the carbons, it is suggested that both an incomplete infiltration of 10X zeolites and the shrinkage of carbon frameworks during the carbonization process will definitely lead to a broad distribution of nanopores with diameters slightly larger than zeolite walls.[23,34] It should be noted that the behavior for small mesopores in carbons is more obvious for the higher temperature sample, that is, the higher temperature favors mesopores and then reduces the zeolite-like structural ordering, surface area, and pore volume. Moreover, as clearly shown in Table 1 and Figure 4, the 10Xc-80 has nearly no pores less than 1.0 nm and possesses much lower surface area than other samples, suggesting that small micropores in carbons have more contributions to the surface area than the larger micropores or mesopores. Although some previous studies have indicated that DFT data for N_2 adsorption is not wholly reliable for micropores because it can overestimate pore size, it must be acknowledged that it is still useful to provide some comparative insights into PSDs.[35,36,40,48] The small difference in the PSDs is fully supported by the information shown in Table 1 that different preparation conditions can greatly affect surface areas and pore volumes. Therefore, adjusting preparation parameters properly is indeed beneficial for obtaining carbons with the sharp PSD curve and high surface area. As also stated in Table 1, 10Xc-70, with the largest surface area and pore volume, also has the highest level of zeolite-like structural orderings evidenced by XRD data in Figure 1. We believe that the special characteristic of 10Xc-70 will definitely exert some positive effects on the hydrogen storage under proper conditions.[11,56] The overall results of PSDs together with XRD patterns and SEM images strongly support a fact that the most micropores of ordered nanoporous carbons are truly replicated from the frameworks of the 10X zeolite template.

Hydrogen sorption isotherms of carbons measured via the gravimetric method at 77 K over a pressure range of 0−20 bar are shown in Figure 5. For the clarity, hydrogen adsorption isotherms for 10Xc60-7S and 10Xc-70S are not shown in Figure 5 due to their very approximate uptakes to 10Xc-75 and 10Xc-60, respectively, which results in difficulty distinguishing each adsorption isotherm. The detailed hydrogen capacities at pressures of 1 and 20 bar are also summarized in Table 1. We found that hydrogen storage uptakes at 77 K and 20 bar for these carbons exhibit an apparent linear relationship with the oxygen element content per surface area (Figure S4, Supporting Information), namely, the existence of oxygen functionalization in carbons has some adverse effects on hydrogen adsorption, which is in good accordance with our previous work.[57] It has been suggested that hydrogen molecules "prefer" adsorbing onto the textural surface of adsorbents via a physisorption mechanism,[32,33,58] and the kinetic equilibrium process for hydrogen in carbons can be achieved rapidly. As can be seen from the inset of Figure 5, hydrogen sorption isotherms for the 10Xc-60 at 1 bar are completely reversible with virtually no

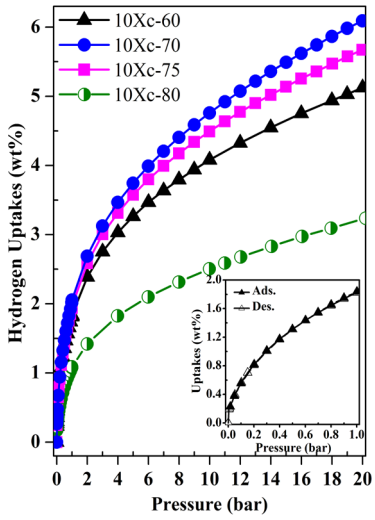

Figure 5. Hydrogen sorption isotherms at 77 K and 20 bar for the zeolite-templated carbons.

hysteresis, confirming that hydrogen adsorption is wholly a physisorption mechanism, and other probable impurities have not been adsorbed in this work.[4,58−61] We further validated that the observed adsorption was due to hydrogen rather than other impurities via the measurement of deuterium isotherms on the same IGA. The comparison gravimetric adsorption results between H_2 and D_2 on the 10Xc-60 as an example were recorded over the range 0−1.0 bar at 77 K and shown in Figure S5 (Supporting Information). It is expected that the mass ratio of adsorbed D_2/H_2 is close to 2:1, and the corresponding molar ratio is nearly in the 1.04−1.09 range, entirely consistent with the values (1.01−1.16) observed in our previous data on the activated carbons.[57,62] Hydrogen storage capacities in carbons at 1 bar varied between 1.1 and 2.3 wt % and the values at 20 bar varied between 3.2 and 6.1 wt %, which are still at a relatively inferior situation compared to previous observations on several activated carbons[41,63] and similar ordered carbons derived from other kinds of zeolites.[29,36−40] Furthermore, it should be admitted that hydrogen uptake for 10Xc-70 is slightly higher than some previously reported data on the carbons templated from other zeolites.[4,30,34,47,51] As we stated above, however, buoyancy effects have great effects on the adsorption results especially for light gas at high pressures; therefore, results for hydrogen adsorption must be subjected to accurate buoyancy corrections. The importance of buoyancy corrections in calculating actual hydrogen storage capacities at high pressures can be illustrated here. Figure S6 (Supporting Information) provides the hydrogen isotherms after buoyancy correction using different corrected parameters, and we can surprisingly note that this correction can affect the hydrogen adsorption capacity with dramatic differences. For example, the hydrogen uptakes on the 10Xc-70 could even reach 8.1 wt % when the corrected density was 0.17 g/cm^3, as suggested by some previous researchers[64] and reach 6.8 wt % when density was 0.34 g/cm^3, whereas the uptake could only reach 4.6 wt % if the corrected density was 1.5 g/cm^3, as adopted in some previous reports.[31,36,40] Moreover, as a representative storage media that relies on physisorption, more and more proof predicts that hydrogen adsorption in the carbon-based materials is proportional to the surface area or pore volume.[65−67] With an increase in pyrolysis temperature from 600 to 700 °C, it can be observed from Table 1 and Figure 5 that these carbons do

exhibit an enhanced hydrogen storage capacity, increasing from 5.1 to 6.1 wt % at 20 bar and 77 K. As the pyrolysis temperature continually increases to 800 °C, however, the capacity rapidly decreases to 3.2 wt % at 20 bar, following the decreasing trend in their textural properties such as the surface areas and pore volumes. Furthermore, the hydrogen uptake on the carbons obtained from liquid−gas two-step routes is similar proportional to the intensity of zeolite-like structure orderings (see Figure 1b,c), demonstrating that the higher intensity of basal peak, the larger surface area of carbons.[20,42] However, we should be note that 10Xc-7S and 10Xc60-7S derived from direct acetylene infiltration also exhibit high hydrogen capacities even if they have relative lower intensity in basal peak (see Figure 1d). Therefore, we hypothesize that this trend for hydrogen storage capacity is closely related to the surface area and porosity of carbons. Several studies have previously indicated that a tight relationship exists between the surface areas and hydrogen uptakes.[48,58,60,65] It is expectable that the carbons with larger surface areas will have more accessible adsorptive sites, resulting in the higher hydrogen storage uptakes, which has been perfectly confirmed in this work. It should be mentioned that the 10Xc-70 has both the largest BET specific surface area and total pore volume up to 3331 m^2/g and 1.94 cm^3/g, respectively, and shows the largest hydrogen storage capacity up to 6.1 wt % at the pressure of up to 20 bar, one of the top-ranked uptakes ever observed in literature for high surface area carbons (Table 1). Furthermore, it is clearly observed that adsorption saturation of all carbons is not achieved even at up to 20 bar, and the larger slope trajectory of isotherm for 10Xc-70 compared with other carbons suggests that a higher capacity can be anticipated at an elevated pressure as the saturation is attained. This superior hydrogen capacity of carbons can be attributed to their excellent pore structures, with large surface area and well-controlled pore size centered at 1.2 nm. Generally, the smaller micropores are better for adsorption below 1 bar, resulting from larger adsorption enthalpy, that is, large interactions between adsorbates and pores. However, for the adsorption at a higher pressure, the larger micropores can also be applicable to play an important role too, which is due to the fact that the higher pressures at larger micropores will moderately reduce interactions between adsorbates and adosrbates, and therefore compensate for the negative effects of larger micropores in adsorption enthalpy.[68−71] That is, the narrower pores at low pressures will increase interactions between adsorbates and adsorbents due to the surface potential overlaps, and therefore the smaller micropores are better for storage below 1 bar. However, this trend will definitely reverse for narrow pores at high pressures where the available surface area for hydrogen storage will play a more significant role.

To understand the relationship between hydrogen storage uptakes and texture properties of carbons, the scattered nature of uptakes at 77 K and 20 bar were plotted versus BET specific surface area and total pore volume (Figure 6). Moreover, the relationship between the DFT specific surface area and hydrogen storage capacity was shown in Figure S7 (Supporting Information). As shown in Figure 6a, the hydrogen storage capacities gradually increase with an increase of surface area for carbons. The hydrogen storage values were also compared to other similar ordered porous carbons inherited from different zeolites under the same conditions. Although the capacities on carbons are proportional to their surface areas and pore volumes, however, we have not observed an absolute linear relationship between the capacities and textural properties. This

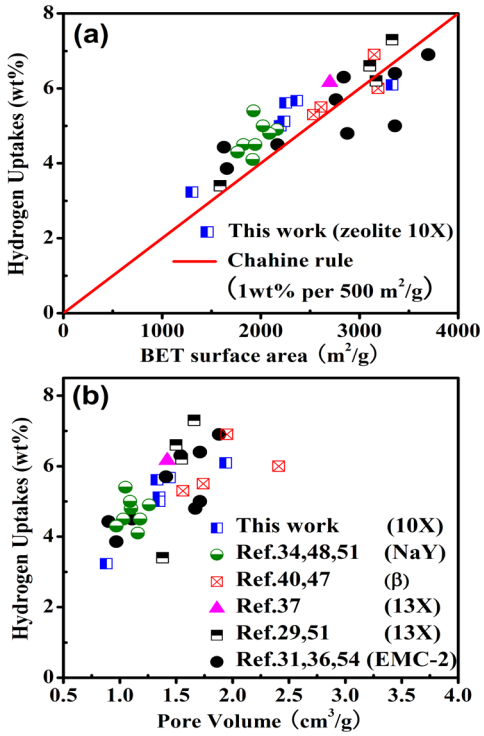

Figure 6. Variation of hydrogen adsorption capacities at 77 K and 20 bar with (a) surface area and (b) pore volume for the ordered porous carbons derived from different zeolites. The line in panel a is a Chahine plot (1 mass % adsorption per 500 m^2/g, converted to wt%).

situation is different from the hydrogen adsorption on some traditional activated carbons, where a better linear correlation between the storage uptakes and surface areas was observed.[2,60,63] The observed linearity in the present carbons can be explained that the pore size effect is not significant enough for these carbons below 20 bar. Moreover, broadening the scope to some other ordered carbons reveals a much more scattered result and we have noted that hydrogen capacities on most of ordered carbons outperform the Chahine rule (i.e., 500 m^2/g of carbon adsorbed 1 wt % hydrogen), especially for carbons with surface areas lower than 3000 m^2/g. It is true that the relationship between the DFT surface areas and hydrogen storage uptakes in Figure S7 (Supporting Information) is also very similar to the situation of BET surface areas. This behavior is due to the presence of a large proportion of pores less than 1.5 nm with narrow PSDs centered at around 1.2 nm in their PSDs.[27,60] Although some previous studies have indicated that the Chahine rule is not always valid,[48,60] it can still serve as an appropriate basis for the cross sample comparison. On the other hand, the 10Xc-75 has a larger surface area and pore volume than the 10Xc60-7S whereas the latter has a slightly higher capacity at 1 bar. We ascribed variations in uptakes to the synergistic effects between PSD and graphitization of carbons. The 10Xc60-7S has a large fraction of microporosity and some ultramicropores at 0.6 and 0.8 nm which are not present in 10Xc-75, indicating that the existence of ultramicropores can make significant contributions to the hydrogen storage uptake at 1 bar because adsorption enthalpy increases dramatically with the decreased distance of pore wall and therefore results in higher hydrogen uptakes. However, the contribution of pores slightly larger than 1 nm in adsorption also should not be ignored because moderate amounts of these

dx.doi.org/10.1021/am403810j | ACS Appl. Mater. Interfaces 2014, 6, 167−175

larger pores may provide fast transportation in carbons and play important roles in hydrogen storage at higher pressures.[66] The sheer magnitude of surface areas and pore volumes can compensate for low capacity efficiency of larger pores to some extent. Moreover, the graphitization of 10Xc60-7S seems to be slightly lower than 10Xc-75. On the basis of the adsorption results, we can infer that the effective micropore size may have a larger effect than the specific surface area at low pressure whereas the surface area can have a larger effect at high pressure. Thus, a proper adjustment of porosity is very necessary to enhance the hydrogen storage capacity, namely, carbons with lower surface areas but proper porosity can also possess high hydrogen capacities. This study also indicates that it is possible to prepare ordered nanoporous carbons with a tailored PSDs and high level of zeolite-like structural ordering using 10X zeolite as a hard template via different precursor infiltration processes. The ability to tailor pores in such a manner within micropore size range is not readily accessible for other forms of carbons.

CONCLUSIONS

In summary, we used zeolite 10X for the first time as a template to nanocast ordered carbons, and the preparation parameters play an important role in determining the levels of structural ordering and textural property of carbons. The structural ordering of carbons from liquid−gas two-step routes is much stronger than the ones from the single acetylene deposition. Carbons have high surface areas (2100−3330 m^2/g) and large pore volumes (0.88−1.94 cm^3/g) with a considerable hydrogen uptake at 77 K, exceeding 6.1 wt % at 20 bar and 2.3 wt % at 1 bar. This storage capacity is in the ranks of the highest values ever observed for large surface area carbons and other porous materials. Our results enriched some insights that are useful for designing suitable carbons for hydrogen storage, and we anticipate that further increases in adsorption capacities can be expected with new carbons possessing similar ordered structures with high surface area and microporosity. Carbons with a high structural ordering and a large surface area maybe have great potential in other fields, although the surface modification is necessary for further enlarging the levels of hydrogen storage under ambient conditions.

ASSOCIATED CONTENT

Supporting Information

N_2 sorption isotherms, TEM images, calculation of BET surface areas, relationship between textural properties and uptakes, comparison of H_2/D_2 isotherms, and H_2 isotherms varied with different parameters for buoyancy correction. This material is available free of charge via the Internet at http://pubs.acs.org.

AUTHOR INFORMATION

Corresponding Author

*X. B. Zhao. E-mail: zhaoxb@qibebt.ac.cn. Tel./Fax: +86-532-80662728.

Notes

The authors declare no competing financial interest.

ACKNOWLEDGMENTS

We greatly appreciate the financial support from "100 Talents Program" of Chinese Academy of Sciences (No. KJCX2-YW-W34) and the National Natural Science Foundation of China (No. 21073216 and No. 21173246).

REFERENCES

(1) Wang, L.; Yang, R. T. *Energy Environ. Sci.* **2008**, *1*, 268−279.
(2) Cheng, F.; Liang, J.; Zhao, J.; Tao, Z.; Chen, J. *Chem. Mater.* **2008**, *20*, 1889−1895.
(3) Cai, J.; Xing, Y.; Zhao, X. *RSC Adv.* **2012**, *2*, 8579−8586.
(4) Guan, C.; Wang, K.; Yang, C.; Zhao, X. S. *Microporous Mesoporous Mater.* **2009**, *118*, 503−507.
(5) Tozzini, V.; Pellegrini, V. *Phys. Chem. Chem. Phys.* **2013**, *15*, 80−89.
(6) Sevilla, M.; Fuertes, A. B.; Mokaya, R. *Energy Environ. Sci.* **2011**, *4*, 1400−1410.
(7) Yurum, Y.; Taralp, A.; Veziroglu, T. N. *Int. J. Hydrogen Energy* **2009**, *34*, 3784−3798.
(8) Schlapbach, L.; Zuttel, A. *Nature* **2001**, *414*, 353−358.
(9) Sevilla, M.; Fuertes, A. B.; Mokaya, R. *Int. J. Hydrogen Energy* **2011**, *36*, 15658−15663.
(10) Masika, E.; Mokaya, R. *J. Phys. Chem. C* **2012**, *116*, 25734−25740.
(11) Nishihara, H.; Kyotani, T. *Adv. Mater.* **2012**, *24*, 4473−4498.
(12) Yang, S. J.; Kim, T.; Im, J. H.; Kim, Y. S.; Lee, K.; Jung, H.; Park, C. R. *Chem. Mater.* **2012**, *24*, 464−470.
(13) Marco-Lozar, J. P.; Juan-Juan, J.; Suárez-García, F.; Cazorla-Amorós, D.; Linares- Solano, A. *Int. J. Hydrogen Energy* **2012**, *37*, 2370−2381.
(14) Xia, Y.; Yang, Z.; Mokaya, R. *Nanoscale* **2010**, *2*, 639−659.
(15) Inagaki, M.; Orikasa, H.; Morishita, T. *RSC Adv.* **2011**, *1*, 1620−1640.
(16) Davis, M. E. *Nature* **2002**, *417*, 813−821.
(17) Kyotani, T. *Bull. Chem. Soc. Jpn.* **2006**, *79*, 1322−1337.
(18) Sakintuna, B.; Yurum, Y. *Ind. Eng. Chem. Res.* **2005**, *44*, 2893−2902.
(19) Zhao, X. S.; Su, F.; Yan, Q.; Guo, W.; Bao, X. Y.; Lv, L.; Zhou, Z. J. *Mater. Chem.* **2006**, *16*, 637−648.
(20) Kyotani, T.; Ma, Z.; Tomita, A. *Carbon* **2003**, *41*, 1451−1459.
(21) Zhai, Y.; Wan, Y.; Cheng, Y.; Shi, Y.; Zhang, F.; Tu, B.; Zhao, D. J. *Porous Mater.* **2008**, *15*, 601−611.
(22) Gadiou, R.; Saadallah, S. E.; Piquero, T.; David, P.; Parmentier, J.; Vix-Guterl, C. *Microporous Mesoporous Mater.* **2005**, *79*, 121−128.
(23) Ducrot-Boisgontier, C.; Parmentier, J.; Delmotte, L.; Patarin, J. J. *Mater. Sci.* **2009**, *44*, 6571−6575.
(24) Ducrot-Boisgontier, C.; Parmentier, J.; Patarin, J. *Microporous Mesoporous Mater.* **2009**, *126*, 101−106.
(25) Liang, C.; Li, Z.; Dai, S. *Angew. Chem., Int. Ed.* **2008**, *47*, 3696−3717.
(26) Song, H. X.; Teo, W. S.; Wang, K. J. *Porous Mater.* **2012**, *19*, 211−215.
(27) Alvarez, S.; Fuertes, A. B. *Carbon* **2004**, *42*, 433−436.
(28) Hou, P.; Yamazaki, T.; Orikasa, H.; Kyotani, T. *Carbon* **2005**, *43*, 2624−2627.
(29) Masika, E.; Mokaya, R. *Prog. Nat. Sci.* **2013**, *23*, 308−316.
(30) Konwar, R. J.; De, M. *Microporous Mesoporous Mater.* **2013**, *175*, 16−24.
(31) Xia, Y.; Zhu, Y.; Tang, Y. *Carbon* **2012**, *50*, 5543−5553.
(32) Stadie, N. P.; Vajo, J. J.; Cumberland, R. W.; Wilson, A. A.; Ahn, C. C.; Fultz, B. *Langmuir* **2012**, *28*, 10057−10063.
(33) Lee, S. Y.; Park, S. J. J. *Colloid Interf. Sci.* **2012**, *384*, 116−120.
(34) Xia, Y.; Yang, Z.; Mokaya, R. *Chem. Vap. Deposition* **2010**, *16*, 322−328.
(35) Sevilla, M.; Alam, N.; Mokaya, R. *J. Phys. Chem. C* **2010**, *114*, 11314−11319.
(36) Xia, Y.; Walker, G. S.; Grant, D. M.; Mokaya, R. *J. Am. Chem. Soc.* **2009**, *131*, 16493−16499.
(37) Wang, H.; Gao, Q.; Hu, J.; Chen, Z. *Carbon* **2009**, *47*, 2259−2268.
(38) Nishihara, H.; Hou, P.; Li, L.; Ito, M.; Uchiyama, M.; Kaburagi, T.; Ikura, A.; Katamura, J.; Kawarada, T.; Mizuuchi, K.; Kyotani, T. *J. Phys. Chem. C* **2009**, *113*, 3189−3196.
(39) Guan, C.; Zhang, X.; Wang, K.; Yang, C. *Sep. Purif. Technol.* **2009**, *66*, 565−569.

(40) Yang, Z.; Xia, Y.; Mokaya, R. *J. Am. Chem. Soc.* **2007**, *129*, 1673−1679.
(41) Chen, H.; Wang, H.; Xue, Z.; Yang, L.; Xiao, Y.; Zheng, M.; Lei, B.; Liu, Y.; Sun, L. *Int. J. Hydrogen Energy* **2012**, *37*, 18888−18894.
(42) Ma, Z.; Kyotani, T.; Tomita, A. *Carbon* **2002**, *40*, 2367−2374.
(43) Kruk, M.; Jaroniec, M.; Gadkaree, K. P. *Langmuir* **1999**, *15*, 1442−1448.
(44) Ravikovitch, P. I.; Neimark, A. V. *Colloids Surf., A* **2001**, *187-188*, 11−21.
(45) Meyers, C. J.; Shah, S. D.; Patel, S. C.; Sneeringer, R. M.; Bessel, C. A.; Dollahon, N. R.; Leising, R. A.; Takeuchi, E. S. *J. Phys. Chem. B* **2001**, *105*, 2143−2152.
(46) Su, F.; Zeng, J.; Yu, Y.; Lv, L.; Lee, J. Y.; Zhao, X. S. *Carbon* **2005**, *43*, 2366−2373.
(47) Pacula, A.; Mokaya, R. *J. Phys. Chem. C* **2008**, *112*, 2764−2769.
(48) Alam, N.; Mokaya, R. *Energ. Environ. Sci.* **2010**, *3*, 1773−1781.
(49) Ducrot-Boisgontier, C.; Parmentier, J.; Faour, A.; Patarin, J.; Pirngruber, G. D. *Energy Fuel* **2010**, *24*, 3595−3602.
(50) Sing, K. S. W.; Everett, D. H.; Haul, R.; Moscou, L.; Pierotti, R. A.; Rouquerol, J.; Siemieniewska, T. *Pure Appl. Chem.* **1982**, *54*, 2201−2218.
(51) Yang, Z.; Xia, Y.; Sun, X.; Mokaya, R. *J. Phys. Chem. B* **2006**, *110*, 18424−18431.
(52) Kyotani, T.; Nagai, T.; Inoue, S.; Tomita, A. *Chem. Mater.* **1997**, *9*, 609−615.
(53) Ania, C. O.; Khomenko, V.; Raymundo-Piñero, E.; Parra, J. B.; Béguin, F. *Adv. Funct. Mater.* **2007**, *17*, 1828−1836.
(54) Xia, Y.; Mokaya, R.; Grant, D. M.; Walker, G. S. *Carbon* **2011**, *49*, 844−853.
(55) Maia, D. A. S.; de Oliveira, J. C. A.; Toso, J. P.; Sapag, K.; López, R. H.; Azevedo, D. C. S.; Cavalcante, C. L., Jr.; Zgrablich, G. *Adsorption* **2011**, *17*, 853−861.
(56) Zhao, W.; Fierro, V.; Zlotea, C.; Aylon, E.; Izquierdo, M. T.; Latroche, M.; Celzard, A. *Int. J. Hydrogen Energy* **2011**, *36*, 5431−5434.
(57) Zhao, X. B.; Xiao, B.; Fletcher, A. J.; Thomas, K. M. *J. Phys. Chem. B* **2005**, *109*, 8880−8888.
(58) Xia, Y.; Yang, Z.; Gou, X.; Zhu, Y. *Int. J. Hydrogen Energy* **2013**, *38*, 5039−5052.
(59) Cygankiewicz, J.; Dudzińska, A.; Żyła, M. *Adsorption* **2012**, *18*, 189−198.
(60) Gogotsi, Y.; Portet, C.; Osswald, S.; Simmons, J. M.; Yildirim, T.; Laudisio, G.; Fischer, J. E. *Int. J. Hydrogen Energy* **2009**, *34*, 6314−6319.
(61) Thomas, K. M. *Catal. Today* **2007**, *120*, 389−398.
(62) Zhao, X.; Villar-Rodil, S.; Fletcher, A. J.; Thomas, K. M. *J. Phys. Chem. B* **2006**, *110*, 9947−9955.
(63) Wang, H.; Gao, Q.; Hu, J. *J. Am. Chem. Soc.* **2009**, *131*, 7016−7022.
(64) Hou, P. X.; Orikasa, H.; Itoi, H.; Nishihara, H.; Kyotani, T. *Carbon* **2007**, *45*, 2011−2016.
(65) Yang, S. J.; Im, J. H.; Nishihara, H.; Jung, H.; Lee, K.; Kyotani, T.; Park, C. R. *J. Phys. Chem. C* **2012**, *116*, 10529−10540.
(66) Xia, K.; Gao, Q.; Song, S.; Wu, C.; Jiang, J.; Hu, J.; Gao, L. *Int. J. Hydrogen Energy* **2008**, *33*, 116−123.
(67) Weng, Q.; Wang, X.; Zhi, C.; Bando, Y.; Golberg, D. *ACS Nano* **2013**, *7*, 1558−1565.
(68) Kowalczyk, P.; Tanaka, H.; Hołyst, R.; Kaneko, K.; Ohmori, T.; Miyamoto, J. *J. Phys. Chem. B* **2005**, *109*, 17174−17183.
(69) Zhao, X.; Xiao, B.; Fletcher, A. J.; Thomas, K. M.; Bradshaw, D.; Rosseinsky, M. J. *Science* **2004**, *306*, 1012−1015.
(70) Luo, J.; Xu, H.; Liu, Y.; Zhao, Y.; Daemen, L. L.; Brown, C.; Timofeeva, T. V.; Ma, S.; Zhou, H. C. *J. Am. Chem. Soc.* **2008**, *130*, 9626−9627.
(71) Okamoto, Y.; Miyamoto, Y. *J. Phys. Chem. B* **2001**, *105*, 3470−3474.